Wear 303 (2013) 154–168

Contents lists available at SciVerse ScienceDirect

Wear

journal homepage: www.elsevier.com/locate/wear

Experimental and analytical thermal study of PTFE composite sliding against high carbon steel as a function of the surface roughness, sliding velocity and applied load

I. Tzanakis [a,*], M. Conte [b], M. Hadfield [a], T.A. Stolarski [c]

[a] Sustainable Design Research Centre, School of Design, Engineering and Computing, Bournemouth University, United Kingdom
[b] IK4-Tekniker, Avenida Otaola 20, 20600 Eibar, Spain
[c] Mechanical Engineering, School of Engineering and Design, Brunel University, Uxbridge, Middlesex, UB8 3BH, United Kingdom

ARTICLE INFO

Article history:
Received 1 August 2012
Received in revised form
1 February 2013
Accepted 26 February 2013
Available online 13 March 2013

Keywords:
Flash temperature
Roughness
Dry sliding wear
Calcium aluminosilicate
Frictional heat
Scroll expander

ABSTRACT

This study investigates the contact temperatures caused by frictional heating of sliding parallel pairs. In this case the materials studied are a PTFE composite in contact with a high carbon steel plate. These materials are commonly used for industrial applications, in particular as the main contacting components within a scroll expander system. The expected contact temperature values are important to be quantified in order to predict failure mechanisms associated with excessive thermal effects caused by sliding friction. A rational and coherent interpretation of the thermal effects on the actual tribological contact is presented.

Contact temperatures are monitored continuously using a high-precision infrared thermal imaging technique with a systematic variation in surface roughness of the high carbon steel material. These surface temperatures are investigated as a function of the friction coefficient, the sliding velocity and the applied load while the most influential parameter for the temperature rise is determined. Analytical results using conventional mathematical methodology are also produced. The analytical and experimental findings are then compared indicating interesting correlations within the macro- and micro-surface temperature regimes and the experimental conditions. Microscopic observations show that thermal effects can seriously affect fibers durability while transfer films formed across the steel counterpart can be beneficial for the operation of scroll systems under specific roughness and test conditions.

1. Introduction

Scroll expander systems are widely used in mechanical applications characterized by dry or lubricated sliding conditions. Typical industrial examples are micro-combined heat and power systems, electrical generators and air-conditioners. Within these applications, scroll devices are utilized and face wear and cavitation are seen. Tzanakis et al. [1,2] has identified the main wear and cavitation mechanisms responsible for the severe damage of the tip seal and the steel plate of a specific scroll expander. Apart from cavitation and sliding wear, frictional heating can also play an important role on the tribological behavior of a scroll expander system.

Frictional heating may cause surface temperatures to reach the melting or softening temperature of polymer materials resulting in a change in friction and wear rates [3,4]. Flash temperatures are generated which are considerably in excess of the bulk and the average temperature of the apparent contact area. This rise of the surface temperature can influence the surface geometry leading to severe local wear and lubrication breakdown. The ability to predict and measure the surface temperatures of the actual contacting bodies is important in order to prevent the failure mechanisms of various tribological components like tip seals. A number of research papers dealing with frictional heating and surface temperatures of various materials under dry and lubricated conditions have been published [5–11] in the recent years. Effects on the applied load, sliding velocity and testing time were most commonly considered. Furthermore, surface roughness parameters are likely to influence the distribution of temperature rise in a sliding contact.

Many studies have shown that the friction coefficient of polymers in rubbing contact with metals decreases with the increment of the applied load and the sliding speed due to the generation of thermal effects in the contact spots [12–15]. An extensive work has been conducted by Persson [16] who developed a theory, which describes the influence of the flash

* Corresponding author. Tel.: +44 077 831 38237; fax: +44 1202 965314.
E-mail addresses: itzanakis@bournemouth.ac.uk, Iakovos.Tzanakis@brunel.ac.uk (I. Tzanakis),

0043-1648
http://dx.doi.org/10.1016/j.wear.2013.02.011

temperature on rubber materials with various roughness profiles including different velocity and load parameters. Additionally Guha and Roy Chowdhuri [17], using a pin on disk apparatus observed that surface temperature for six different roughness pairs of sapphire pin against a steel disk increases monotonically with roughness. Moreover Chang and Friedrich [18], using a similar configuration investigated the influence of TiO_2 nano-particles in the wear and thermal behavior of four different pairs of short fiber-reinforced polymers (SFRP). Chang has shown that the surface roughness of the SFRP significantly increases with the increment of pressure velocity product PV until a certain value (6 MPa m/s) is reached; beyond this point the value slightly drops. In contrast the temperature on the counterface steel disk gradually increases with the PV parameter. Thus no direct correlation between thermal effects and roughness parameters can be effectively drawn. Generally, the thermal behavior of sliding bodies is a multi-complex issue and it is widely recognized that the friction processes are not well understood.

In general, within the rubbing surfaces, the sliding bodies dissipate heat and the temperature falls. However, within a damaged area of a polymer the dissipation of heat is more difficult and the temperature significantly increases reducing the cohesive energy of the material [19]. Consequently cracks and deep grooves are developed across the surfaces leading to the wear debris formation. The PV limit, which is the upper limit of acceptable operating conditions for plastic materials, is directly correlated with the generation of frictional heat, the thermal deformation of the actual contact and the wear behavior of the materials. Lancaster [20] showed that the PV limit is in reality a critical surface temperature limit. Tzanakis et al. [21] highlighted the importance of the PV limit in a lubricated sliding contact of a scroll expander unit. These results indicate that the viscoelastic behavior of a tip seal similar to that in this study can be significantly affected and the resulting friction can be altered due to the adhesion product formation.

In this study, the main objective is to understand how the surface temperatures, which are generated by the combination of various surface profiles, sliding velocities and applied loads, affect the studied tribo-pair. Thus a combination of experimental methods and analytical findings which provide an in depth understanding of the heat generation mechanism during the specific friction regime is used. Analytical results using the thermal models of Bowden and Tabor [22] show very good agreement with the experimental macro-contact temperature results and the microscopic observations of the thermally deformed fibers and worn areas.

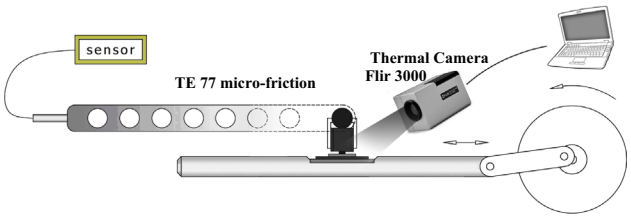

Fig. 1. Schematic of the experimental test rig.

2. Experimental procedure

2.1. Microfriction infrared experiment

The experimental test rig used for this study is described in Fig. 1. The TE 77 micro-friction machine operates by sliding a lower-plate sample (high carbon steel) with a reciprocating motion in contact against a fixed sample pin (tip seal). A pin is connected via a feedback mechanism to a transducer to provide friction force feedback. A high precision infrared camera (Flir 3000) was installed at a distance (10 cm) close to the concentrated contact. This thermal camera has a working temperature range of −20 °C to +2000 °C with an accuracy of ±1% or 1 °C for measurement ranges of +150 °C maximum. The system has a thermal sensitivity of 20 mK at 30 °C and a spectral range of 8–9 μm with a

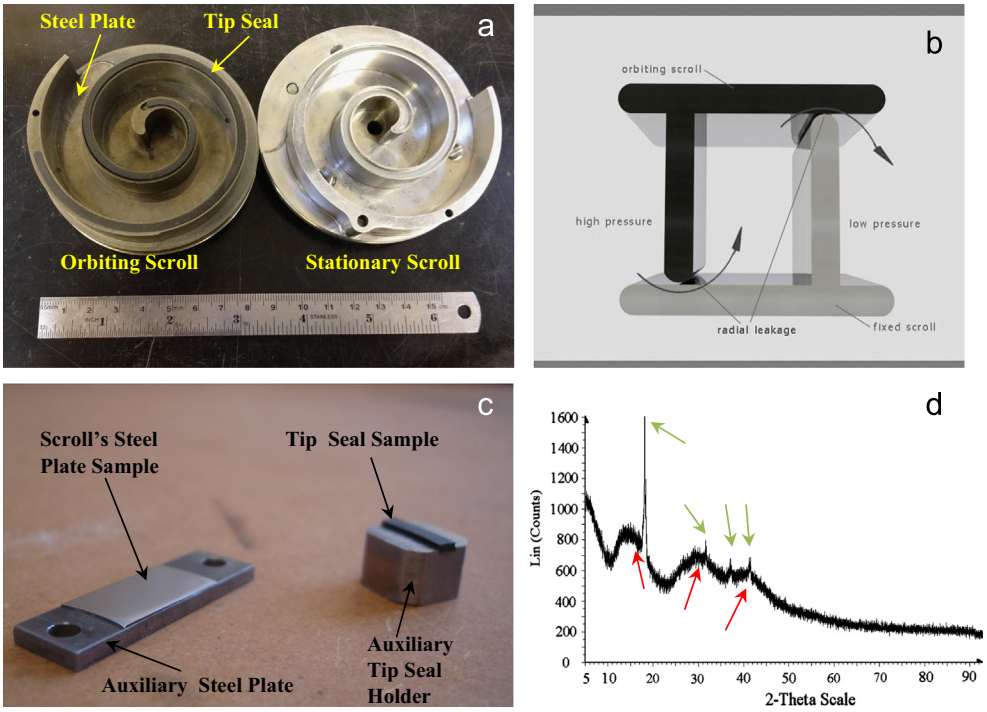

Fig. 2. (a) The scroll expander system disassembled. (b) Schematic of the leakage gaps. (c) Test samples. (d) X-ray diffraction pattern of the tip seal sample. (For interpretation of the references to color in this figure legend, the reader is referred to the web version of this article.)

resolution of 320×240 pixels. Calibration was carried out in agreement with the procedure described in the instructions for use of the FLIR ThermoCamera. The primary interest was to minimize the reflected energy from the surrounding materials in the vicinity of the contact. Thus, most of the metallic parts of the test rig were insulated ensuring that precise temperature measurements will be achieved. Friction and thermal results at the contact points were analyzed during post-test analysis using the camera's software.

This experimental set-up using a TE 77 micro-friction tribometer enabled a continuous reciprocating surface contact. The reciprocating tribometer simulates the kinematic motion of the industrial scroll's expander system. Thermal energy, which is not removed from the interface, raises the temperature locally. The infrared camera measures the heat radiation of the frictional contact surface, which is dissipated from the edges of the contact. In contrast, in the pin-on-disk experiments the cooling effects of the pin play a more important role in thermal calculations as heat can be released from the track between passes. Thus, the measurements of contact temperatures using the TE 77 infrared test rig are more accurate.

2.2. Test samples and preparation

The scroll is a device that uses two interleaved spiral shaped scrolls to compress or to expand fluids (Fig. 2a). In the areas across the tip seal and the steel plate contact, where frictional wear is excessive, leakage path (radial leakage) can be developed from tiny micro-gaps which are formed between the bottom or the top steel plate and the scrolls (Fig. 2b). The efficiency of the scroll can be significantly affected. Several sets of laboratory tests utilizing the tip seal and the steel plate of the scroll were conducted to study the friction mechanisms and the surface temperature rise of the tested samples (Fig. 2c).

The steel plate sample is a high carbon steel material (0.95% carbon) with a length of 15 mm and 0.3 mm thickness and it has a thermal conductivity of 50 W/mK, thermal diffusivity of 1.4×10^{-5} m^2/s and a hardness of 530 HV. Its mechanical properties and chemical composition can be found in [4]. The surface quality of the steel plate samples is achieved by surface grinding, lapping and fine polishing (down to 1 μm polycrystalline diamond suspension in combination with colloidal silica suspension for final polishing). The steel samples are carefully selected according to the surface profile measurement using a ZYGO optical interferometer and then cleaned with acetone and dried. The repeatability and reproducibility have also been considered. The repeatability has been verified by performing 10 times the same measurement on the same surface at different locations (each location/area was 5 mm^2). The reproducibility has been tested by producing samples with similar and uniform roughness profiles. The composite tip seal is a PTFE material reinforced with a combined structure of randomly oriented short fibers made by amorphous man-made mineral fibers (MMMF) calcium aluminosilicate (with chemical formula $CaAlSi_3O_5$). Use of calcium aluminosilicate as fillers in the making of PTFE matrix composites or other similar polymers can reduce the density of the composite material while maintaining or increasing their strength, making these light-weight composites very desirable for industrial applications [23].

The fiber's chemistry and morphology were characterized by using a Zeiss Supra 35VP FEG-SEM for energy-dispersive X-ray analysis (EDX) and crystallinity was investigated using a Bruker D8 Advance X-ray diffractometer with Bragg–Brentano geometry. The XRD spectrum identified peaks (green arrows) of PTFE material while the amorphous peaks (red arrows) belong to the MMMF calcium aluminosilicate fibers (Fig. 2d). The tip seal has a thermal conductivity of 0.4 W/mK, thermal diffusivity of 1.85×10^{-7} m^2/s, a roughness of 3.2±0.4 μm and a hardness of 5.2±0.1 HV while the fiber sizes vary from 50 to 100 μm having a diameter of about 8–10 μm, thermal conductivity of 1.6±0.1 W/mK and a hardness of 865±25 HV [24]. Bulk PTFE has a transition phase between 10 and 30 °C; above 30 °C the material converts into a pseudo-hexagonal disordered phase from a partially ordered hexagonal phase. Thus, thermal diffusivity temperature dependence above 25 °C is small. Conte et al. [25] explain how this transition phase can be considered as the main cause of the transfer layer mechanism at the running in stage. The nominal area of contact of the tip seal

Table 1
Measured and calculated contact temperature results according to the frictional contact regime (PTFE/steel plate) and (Fiber/steel plate) of the steel plate with the composite tip seal for four different steel roughness profiles under various contact pressures and sliding velocities.

Roughness (μm)	Pu factor (MPa, m/s)	Friction coefficent	Measured	Calculated	
			Contact temperature (°C)	Contact temperature (°C)	
			FLIR camera	PTFE/steel plate	Fibers/steel plate
0.125	0.8 MPa, 0.25 m/s	0.15	47.1	51.7	270.0
	1.6 MPa, 0.25 m/s	0.13	61.5	62.4	329.9
	0.4 MPa, 0.5 m/s	0.22	52.6	76.7	529.4
	0.8 MPa, 0.5 m/s	0.21	74.4	95.4	706.5
	1.2 MPa, 0.5 m/s	0.19	87.3	109.2	786.3
	1.6 MPa, 0.5 m/s	0.175	96.6	111.2	831.4
0.25	0.8 MPa, 0.25 m/s	0.19	52.7	56.9	333.3
	1.6 MPa, 0.25 m/s	0.16	75.8	63.4	392.7
	0.4 MPa, 0.5 m/s	0.24	55.8	80.5	574.4
	0.8 MPa, 0.5 m/s	0.23	84.3	101.6	770.9
	1.2 MPa, 0.5 m/s	0.22	102.6	115.4	899.5
	1.6 MPa, 0.5 m/s	0.21	114.8	126.8	991.0
0.5	0.8 MPa, 0.25 m/s	0.13	39.6	46.3	235.4
	1.6 MPa, 0.25 m/s	0.11	52.7	50.8	277.1
	0.4 MPa, 0.5 m/s	0.19	48.4	70.5	461.4
	0.8 MPa, 0.5 m/s	0.14	56.1	69.8	477.2
	1.2 MPa, 0.5 m/s	0.15	73.8	85.4	620.0
	1.6 MPa, 0.5 m/s	0.14	81.8	91.0	667.2
0.7	0.8 MPa, 0.25 m/s	0.12	41.7	48.2	222.8
	1.6 MPa, 0.25 m/	0.10	53.2	50.8	256.6
	0.4 MPa, 0.5 m/s	0.18	44.9	68.5	438.8
	0.8 MPa, 0.5 m/s	0.15	57.6	77.8	514.3
	1.2 MPa, 0.5 m/s	0.15	73.0	88.0	622.6
	1.6 MPa, 0.5 m/s	0.14	79.2	91.9	668.1

samples over the steel plate is 25 mm^2. Prior to any test tip seal samples were merged into boiling water for 30 min in order to be thoroughly cleaned from any undesirable surface contaminants like dirt or dust.

2.3. Test conditions

Experiments were carried out using velocity and load conditions in close proximity with those in the actual scroll expander system as in [4]. Two different sliding speeds were used at 0.25 and 0.5 m/s and a contact force of 10, 20, 30 and 40 N is applied. Additionally, four different Ra profiles of the steel plate with a mean value of 0.125±0.015, 0.25±0.025, 0.5±0.04 and 0.7±0.05 μm were used in order to investigate the influence of the Ra profile to the contact temperature rise. The run-in time period is 600 s since it has been seen that steady state thermal effects are developed within that time [26]. Specifically, during previous measurements of 30 and 60 min it was found that after a lapse of 10 min the contact temperature on the surface of the rubbing samples stabilizes and so equilibrium of the heat generated inside the sample with the environment is achieved. The average increment of the contact temperature (percentage change) after the first 10 min is in the order of 3%, indicating an average temperature increment of 2 °C for each case and implying that significant changes in the thermal regime are restricted for a prolonged period of time. This was achieved by correlating the results of [26] and the results of preliminary tests conducted for the purpose of this research. This was calculated using the following expression:

$$I_T(\%) = \frac{|T_S - T_P|}{T_S} \times 100 \quad (1)$$

where I_T is the average percentage of increment (percentage change) of the contact temperature after the initial running-in stage of 10 min, T_S (°C) is the temperature over the initial period of time i.e. 10 min and T_P (°C) is the temperature over a prolonged period of time i.e. 30 or 60 min. All the tests were performed under dry sliding condition and an ambient temperature environment with temperature at 23±1 °C and humidity levels at 50%. In all the experiments the pre-test contact temperature when samples were at rest was varied within the range of 28±3 °C according to the applied load and the roughness profile.

3. Experimental results

A number of experiments using different combinations of applied pressure, sliding speed and surface roughness were carried out (Table 1). A thermal image (Fig. 3) of a measurement, along the longitudinal direction of the steel plate counterpart, shows the temperature field. The higher temperature areas are clearly visible across the contact surfaces showing a tendency of the frictional heat to be accumulated within the mass of the polymer bulk material. The temperature of the tip seal sample is aggravated since thermal effects dominate and soften the contact while the poor thermal conductivity and diffusivity of the polymer restrains the dissipation of the accumulated frictional heat.

The thermal behavior of the rubbing materials was evaluated by a series of temperature and friction graphs (Figs. 4–9). The graphs show the relationship of the contact temperature with the sliding time, distance and friction coefficient for different applied loads, sliding speeds and roughness profiles. In order to obtain meaningful and comparable data a repeatable test regime was required. Thus, each result is an average value of at least three experimental data and the scatter in data was within ±10%.

In Figs. 4–9 it can be seen that the friction coefficient increases rapidly, in the very first stage of the sliding test while it then stabilises to a steady-state level when thermal effects become active. The thermal effects cannot be instantaneously generated, softening the substrate of the polymer, thus contact is more severe initially. Then transfer films are formed alleviating the contact. After transfer layers are removed the temperature is significantly increased until another layer is formed. Every time the film thickness is removed friction coefficient is increased due to the severe contact between the fibers and the steel surface while the contact temperature gradually increases until it stabilises after the end of the running-in stage (first 10–30 s) where thermal effects dominate and a steady friction regime is achieved. As the velocity and load increases thermal effects are elevated and the real contact area between the contact bodies tends to increase due to thermal expansion of the polymer. Consequently, hot-spots are multiplied leading to higher contact temperature values. In the case where higher roughness profiles were used the frictional and thermal effects are alleviated. Steel samples with 0.7 and 0.5 μm Ra roughness profile exhibit significantly lower friction coefficients than the 0.25 and 0.125 ones. Correspondingly the thermal effects are also lower.

Figs. 4 and 5 present the variation of frictional coefficient and contact temperature over the sliding distance and the testing time for four roughness steel profiles 0.125, 0.25, 0.5, and 0.7 μm under two applied load levels at 20 and 40 N and sliding velocity at 0.25 m/s. It can be seen that for both cases the 0.25 μm roughness profile exhibits the highest friction coefficient as well as contact temperature followed by the 0.125 μm Ra profile while the remaining higher Ra profiles of 0.5 and 0.7 μm show similar frictional and thermal behavior. Specifically with the increment of the applied load from 20 N (0.8 MPa) to 40 N (1.6 MPa) friction coefficient is slightly reduced especially for the lower Ra's while

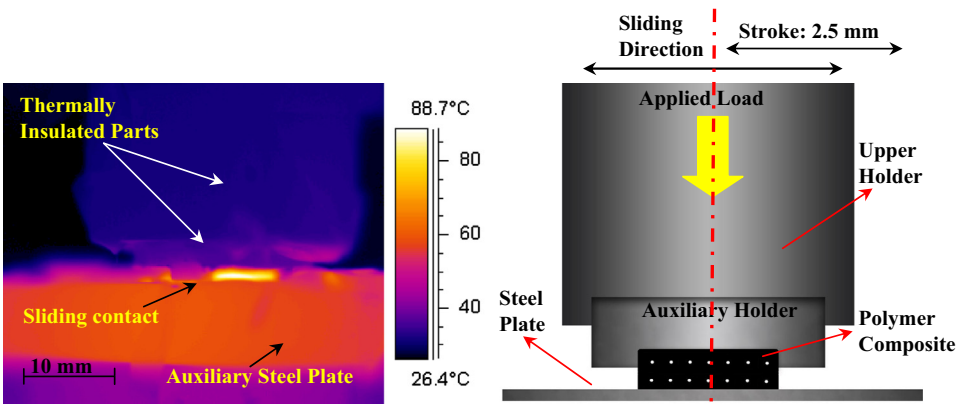

Fig. 3. (a) Real time measurement with thermal camera across the line contact of the tested samples. (b) Sketch of the configuration.

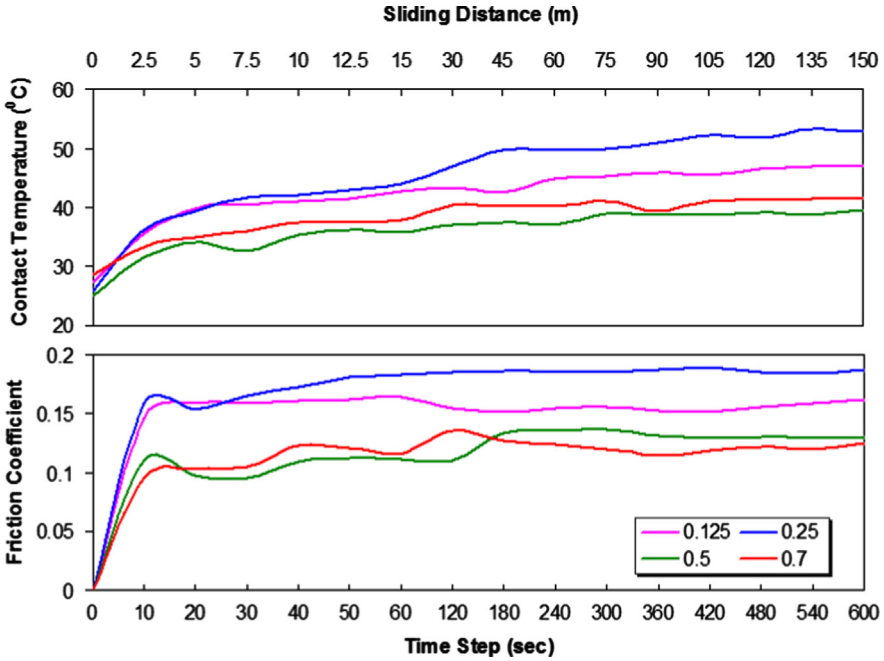

Fig. 4. Comparison of the frictional process (frictional coefficient and contact temperature) of the steel/polymer dry contact for various roughness profiles (0.125, 0.25, 0.5 and 0.7 μm) under an applied pressure of 0.8 MPa and sliding velocity of 0.25 m/s.

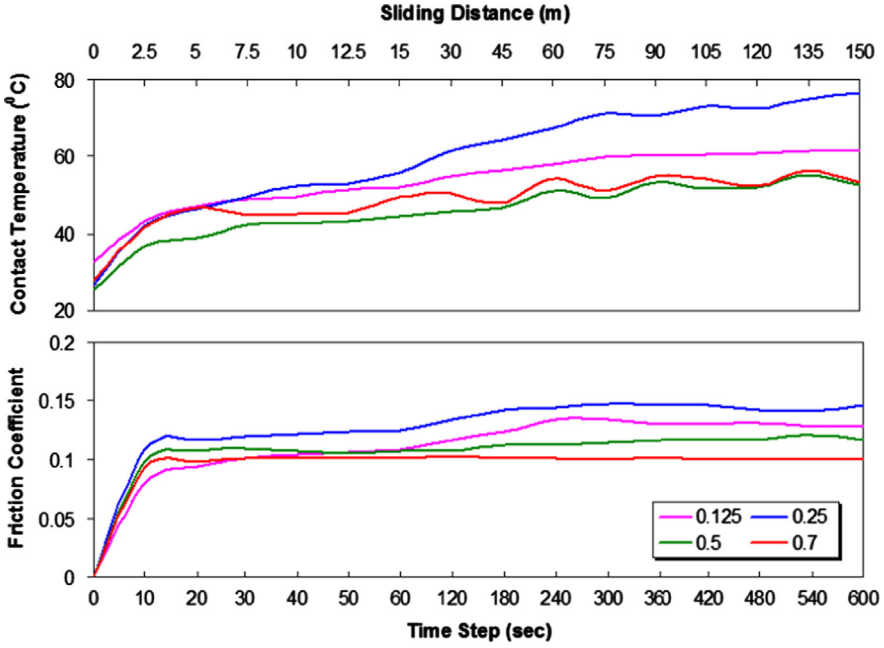

Fig. 5. Comparison of the frictional process (frictional coefficient and contact temperature) of the steel/polymer dry contact for various roughness profiles (0.125, 0.25, 0.5 and 0.7 μm) under an applied pressure of 1.6 MPa and sliding velocity of 0.25 m/s.

contact temperature is significantly increased. This is something that was expected to be seen, since due to the excessive thermal effects by the increment of the applied load, the viscoelastic behavior of the tip seal smoothens the contact and thus friction coefficient drops. On the contrary, the real contact area increases accumulating more frictional heat leading to higher contact temperatures. Interestingly, something which was not expected to be seen is that maximum thermal effects for both cases were recorded when roughness was at 0.25 μm.

In Figs. 6–9 the variations of friction coefficients and contact temperatures are presented as a function of the distance for sliding velocities of 0.5 m/s. Four different applied loads at 10, 20, 30 and 40 N were used under the same roughness profiles as in Figs. 4 and 5. In this series of graphs it can be noted that contact temperature increases with sliding speed and the applied pressure whereas friction coefficient drops with the increment of load as viscoelasticity dominates. In general for all the graphs, an increment of friction coefficient indicates an immediate increment of the contact temperature. The contact temperatures reach higher values i.e. 118 °C in the case of the 40 N applied load (1.6 MPa), accelerating the shearing mechanism of the polymer tip seal. Since the glass temperature of the polymer is in the range of 120–130 °C a surface film with different thermal and mechanical properties than those of the substrate is likely to be developed due to shearing and

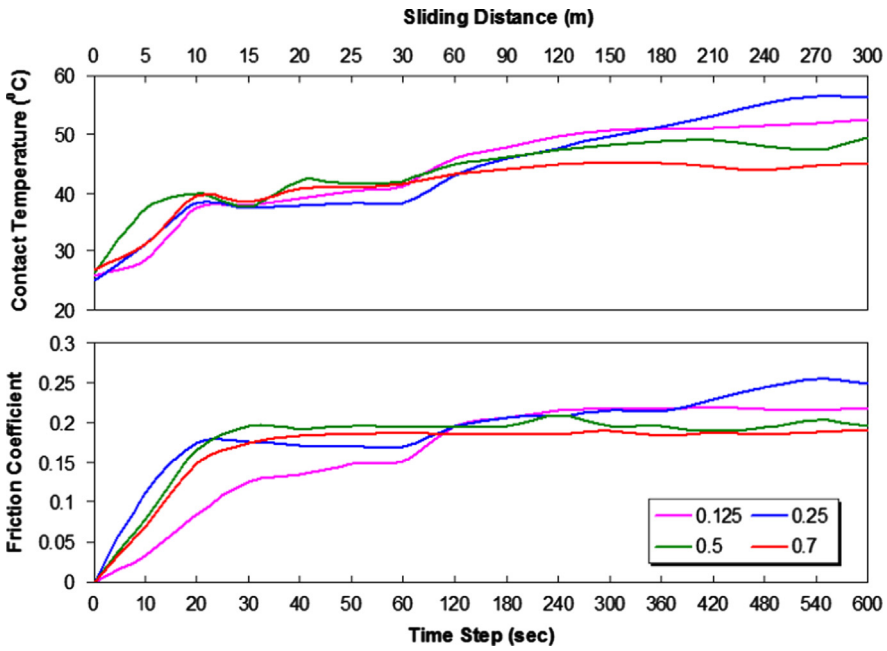

Fig. 6. Comparison of the frictional process (frictional coefficient and contact temperature) of the steel/polymer dry contact for various roughness profiles (0.125, 0.25, 0.5 and 0.7 μm) under an applied pressure of 0.4 MPa and sliding velocity of 0.5 m/s.

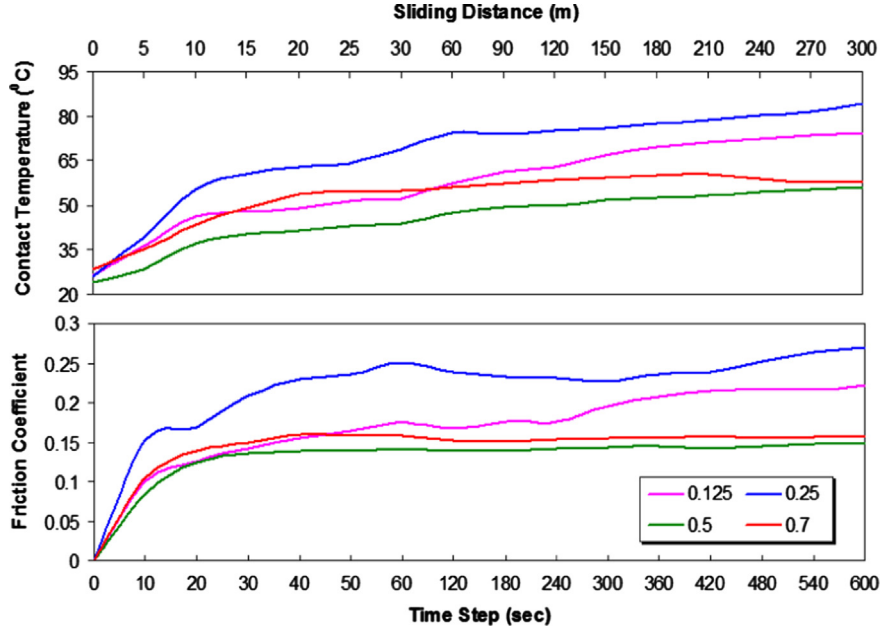

Fig. 7. Comparison of the frictional process (frictional coefficient and contact temperature) of the steel/polymer dry contact for various roughness profiles (0.125, 0.25, 0.5 and 0.7 μm) under an applied pressure of 0.8 MPa and sliding velocity of 0.5 m/s.

seizure of the polymer material. Consequently, a transfer film layer having a dual role of acting as a cushion and as a thermal insulator will not only affect the coefficient of friction, but also the dissipation of thermal energy. The transfer film accumulates frictional heat within the rubbing surfaces while simultaneously reducing friction coefficient values.

Once again the contact regime with Ra at 0.25 μm generates the higher contact temperature values among all the studied cases. It seems that there is a specific roughness profile where the particular contact regime generates excessive thermal effects. The initial idea was that this could be due to the accumulation of larger number of transfer films in that particular Ra profile affecting the frictional heat dissipation rate; however since the contact temperature increases according to friction coefficient this cannot be the case. Thus it can be explained by the combined performance of the steel asperities and the transfer films formation. In the case where Ra is at 0.25 μm transfer films are not so effective allowing more contact within the steel asperities and the reinforced polymer compared to the case where Ra is at 0.125 μm where transfer films create a thicker cushion layer in between the rubbing materials avoiding excessive asperity contact. On the contrary, in the cases with higher Ra values, 0.5 and 0.7 μm, transfer films are limited but substantially thicker across the contact zones of the highest surface asperities. This particular mechanism alleviates severe contact reducing the friction force while as the real average distance of two sliding surfaces is higher air layers can be trapped within the contact zones cooling down the contact. Therefore, the evolution of the roughness of the

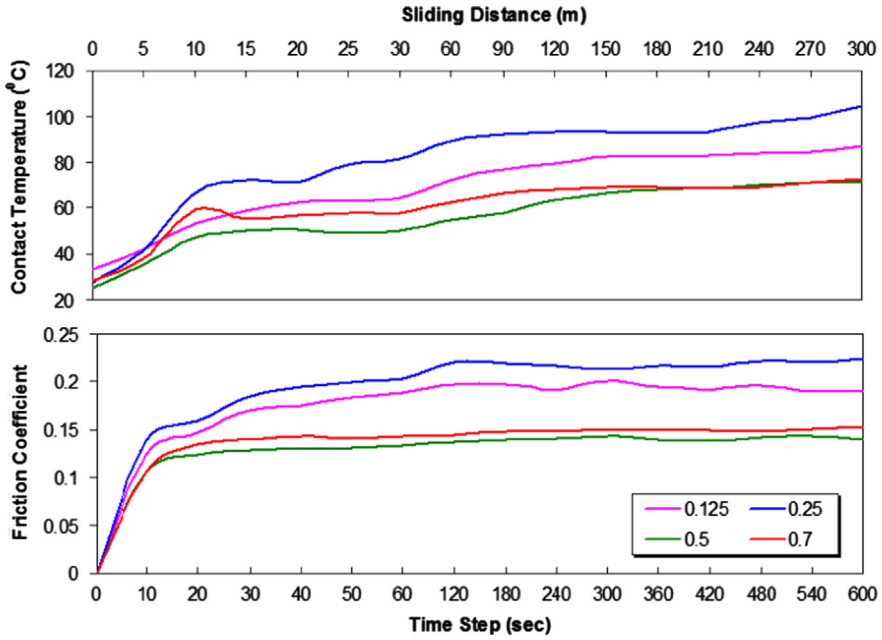

Fig. 8. Comparison of the frictional process (frictional coefficient and contact temperature) of the steel/polymer dry contact for various roughness profiles (0.125, 0.25, 0.5 and 0.7 μm) under applied pressure of 1.2 MPa and sliding velocity of 0.5 m/s.

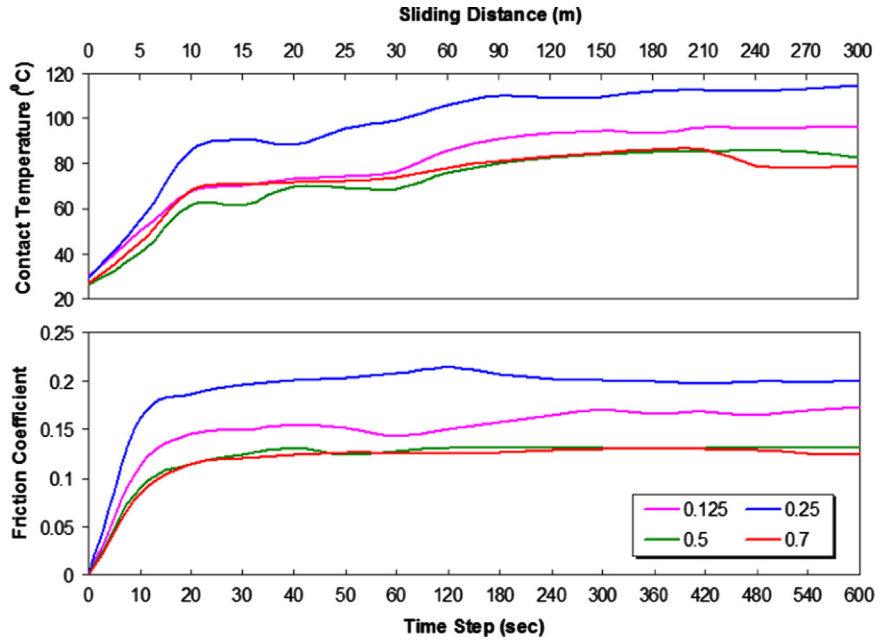

Fig. 9. Comparison of the frictional process (frictional coefficient and contact temperature) of the steel/polymer dry contact for various roughness profiles (0.125, 0.25, 0.5 and 0.7 μm) under an applied pressure of 1.6 MPa and sliding velocity of 0.5 m/s.

counterface plays a significant role along the traveled distance. However a direct correlation between roughness profile and contact temperatures cannot be effectively drawn.

In Fig. 10 the contact temperature under different roughness profiles was plotted against the rate of specific frictional work in order to further understand the correlation between these three parameters. The rate of specific frictional work W_f is defined as

$$\dot{W}_f = \mu P u \ (\mathrm{Nm/m^2 s}) \tag{2}$$

where μ is the frictional coefficient, P is the applied pressure (MPa) and u is the sliding velocity (m/s). It is clear that for all the cases the contact temperature is almost linearly proportional to the rate of frictional work. The highest surface temperature values are measured when roughness profile was at 0.25 μm followed by the 0.125 μm, then the 0.5 μm and finally the 0.7 μm. Interestingly it can be seen that as the roughness increases or decreases from 0.25 μm, contact temperatures are alleviated significantly when roughness doubled up to 0.5 μm and less significantly when it doubled down to 0.125 μm. The influence of the roughness on the actual contact temperature can be clearly observed when a random area on the graphs of Fig. 10 is considered i.e. rate of specific frictional work at 0.1×10^6 Nm/m^{2}s. In that area surface temperatures for all the cases are nearly 80 °C; however for the contact with roughness 0.25 μm, contact temperature is achieved using significantly lower PV factor combinations in comparison to the rest of the cases where higher PV factors are requested (Table 1). The reason is that in the 0.25 μm roughness case, higher friction coefficient rates are generated under the same PV factors

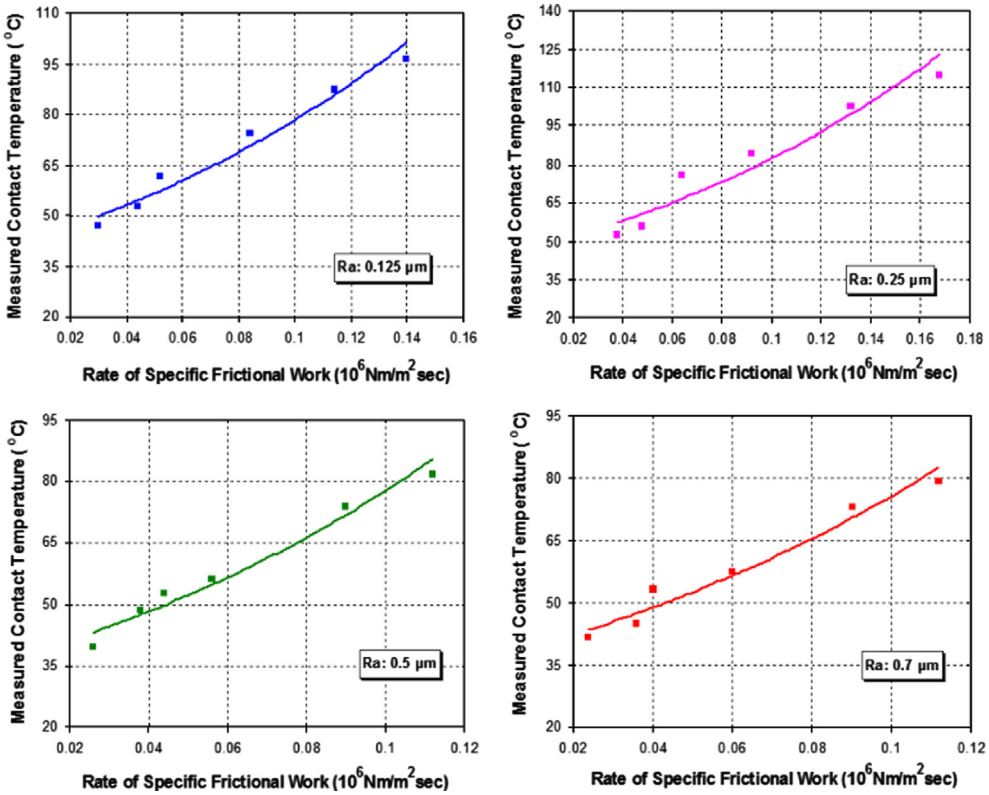

Fig. 10. The steady state experimentally measured contact temperature against the steady state rate of specific frictional work under various roughness profiles.

leading to higher surface temperatures. It seems that for the specific roughness profile hot-spots are significant while the absence of third particle mechanisms in combination with the inefficient cooling performance by the transfer films cannot alleviate severe frictional contact. Additionally as roughness moved further up from 0.5 to 0.7 μm insignificant changes to the contact temperatures were recorded.

A comparison of the tested parameters was conducted in order to evaluate their impact factor on the surface temperature values. Figs. 4–9 reveal the influence the sliding velocity, applied pressure and surface roughness has on contact temperature and frictional coefficient. In Fig. 11, results indicate the percentage of influence of the same parameters on the generation of thermal effects. The higher the percentage, the greatest the impact on the contact temperature regime. For all the cases two out of the three parameters were kept steady while the remaining one was doubled (except in the last case of roughness, which went from 0.5 to 0.7 μm). Consequently, the influence which individually each parameter has on the actual contact temperature is revealed. Contact temperature is significantly influenced by the sliding velocity rather than the applied load and surface roughness. Sliding velocity has the biggest share on the pie chart with 51.3% of influence on the contact temperature regime which means that if the sliding velocity is doubled the surface temperature correspondingly is almost doubled as well. It could be explained considering that the higher the sliding velocity, the shorter the exposition time of free surface to the environment with subsequent less heat dissipation. Then contact pressure follows which exhibits a steady performance for both cases, around 35%. This again shows that if applied pressure is doubled contact temperature is increased at around one-third from the initial value. In contrast to the applied pressure the impact of the roughness profile varies more significantly showing a discrepancy of the percentage of influence. The alteration of roughness profile from 0.25 to 0.5 μm revealed a high influence on the contact temperature regime about 29.4%. Interestingly, this is the only case where surface temperature is

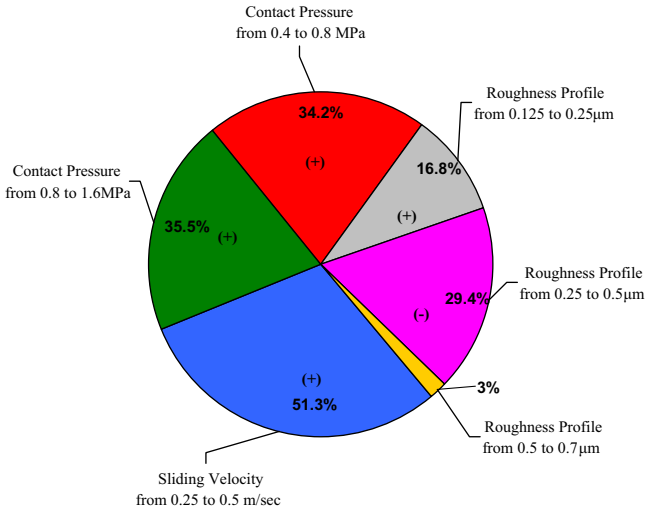

Fig. 11. Percentage of influence of the sliding speed, applied pressure and roughness profile on the generation of contact temperatures across the steel/polymer dry contact. Plus indicates an increase and minus a decrease on the contact temperature regime.

declined, in a similar rate (about one third) to that of the applied pressure. In contrast, in the case where the roughness changed from 0.125 to 0.25 μm the percentage of influence is significantly lower to around a half at 16.8% showing an increment of the contact temperature while when roughness increased from 0.5 to 0.7 μm the influence was almost negligible. Thus it can be deduced by comparing the influence of each parameter in the friction regime that sliding speed plays an overwhelming role in local heating and the determination of surface contact temperatures, followed by the applied pressure and finally the evolution of the roughness of the counterface.

4. Theoretical contact temperature

The system of interest for the studied contact is the surface of the PTFE composite sliding against the high carbon steel plate. Two are the case studies, which were developed for this particular contact. The first one investigates the contact temperature between the bulk material of the polymer composite and the steel surface, the so called macro-contact, while the second one examines the generation of contact temperatures between the MMMF calcium aluminosilicate fibers and the steel asperities, the so called micro-contact. The maximum surface contact temperature is calculated.

$$T_{Contact} = T_{bulk} + T_{flash} \quad (3)$$

where T_{bulk} is the bulk temperature of the sample before entering the contact (28±3 °C) and T_{flash} is the flash temperature. Flash temperature is generated due to frictional heat and is reached for a very short time at the contacting asperities during sliding. There are two types of thermal models in order to calculate flash temperatures. The first one takes into account the dimensions of the surfaces in contact while the second one considers only the material properties neglecting the geometrical profile of the contact. The first type of models is represented by the thermal models of Blok, Jaeger, Ashby et al., Tian and Kennedy [27–30] and the second one by Bowden and Tabor [22]. The above models predict the magnitude of flash temperature from certain input data. However experimental validation of these models often shows that there is a big discrepancy between the measured and the calculated values. For the purposes of this analysis, as in nearly all frictional heating situations it is assumed that the steady-state (or quasi-steady-state) conditions prevail and all frictional energy is dissipated as heat within the contacting bodies at the actual contact interface, producing temperature rise.

In this study both of the numerical approaches were used; however only the Bowden and Tabor (Eq. 4) model worked well for the specific contact [31].

$$\Delta T = 0.443 \ \frac{g\mu V(WP_m)^{1/2}}{J(k_1+k_2)} \quad (4)$$

where ΔT is the flash temperature (°C), g is the acceleration constant (9.81 m/s^2), μ is the dynamic friction coefficient, V is the sliding speed (m/s), W is the contact load, P_{m} is the hardness of the softer material (MPa), J is the mechanical equivalent of heat (4.186 J) and k_1 and k_2 are the thermal conductivities of the contacting materials (W/mK).

Bowden and Tabor's equation takes directly into account the work done by the friction force, considering just the shape of the contact area where Hertz's theory is applied. Blok, Jaeger, Asbhy, Tian and Kennedy equations are explicitly dependent on the dimensions of the contact area. Bowden and Tabor's equation puts the attention to the thermal and mechanical characteristics of the rubbing materials and to the importance of velocity and friction (both enter at the first power into Bowden's equation). Considering the hardness of the softer material Bowden's equation permits a direct correlation with Hertz's theory for calculating the theoretical contact area and the maximum contact pressure. Additionally, according to Persson's investigation [16], due to the strong temperature dependence of viscoelastic properties of rubber-like material, local temperature calculation should be taken into account in order to explain the frictional behavior of the tribo-pair. Considering the thermal behavior of polymers, for example by means of differential scanning calorimetry (DSC), it is possible to affirm that PTFE structure changes when heated up, increasing thermal stability and degree of crystallinity of the matrix due to the release of volatile components, the movement of polymeric chains and a possible secondary bonding effect between the fibers and the matrix [32]. The latter phenomenon, in particular, affects the crystalline structure as observed by Conte et al. [33] where the small crystals are broken and re-generate the transfer layer. The bulk material has a more compact structure where fillers are interposed between big crystals and aligned polymeric chains suspended in the amorphous phase. Thus, it is still possible to approximate the real contact area with the nominal contact area, using again the Bowden and Tabor's equation for the thermal asperity calculations.

Initially, the theoretical flash temperature using the macro-asperity contact of the sliding units is determined. In a polymer contact is rather vague to use the term flash temperature as the polymer does not have required hardness to generate truly flash temperature in a sliding contact; thus the term “interface temperature” is used instead. Interestingly, the calculations were shown (Table 1) that in most of the cases the interface temperature of the macro-asperity contact correlates very well with the real time recorded thermographic results. Specifically, there is a good agreement in general between the calculated results and the experimental results measured with the IR camera. However, in some cases calculations reveal a small discrepancy of the contact temperature results compared to the real time measurements, especially when lower loads were applied. This is due to the fact that the thermal models like the Bowden and Tabor are focused on the interface and not on the thermal impedance of the surrounding equipment like heat flow into the fixtures, forced convection and radiation. Thus, as the real area of contact is reduced, the surrounding air environment, which is trapped within the contact bodies, plays an important role in alleviating thermal effects.

In the case where the micro-asperity contact was taken into consideration an attempt to determine the rise of the flash temperature by the asperities contact of the MMMF calcium aluminosilicate fibers against the asperities of the steel plate is performed. As far as interface temperature is well predicted by the Bowden and Tabor model for the particular macro-contact of the composite with the steel, it is assumed that the specific thermal model will work equally well with the micro-contact between the steel asperities and the exposed fibers. After a running-in period, that is, after the formation of a transfer layer on the steel countersurface, the roughness of the hardest part is attenuated and furthermore, the fibers are sliding partially on PTFE and partially on the steel. For the purpose of this analysis only the contact between the steel asperities and the fibers is considered since the contact between the transfer films and the fibers is hardly appropriate to calculate due to the viscoelastic effects and the transient nature of the transfer films.

The calculations in Table 1 show that flash temperature in micro-asperity contact rises nearly to 1000 °C in the case where roughness is at 0.25 μm and 830 °C when it is at 0.125 μm in contrast to the case where roughness was at 0.5 and 0.7 μm and temperature went up to 670 °C. These temperatures can become critical for the operation of scroll expanders or similar automotive industrial units since heat can be carried away by lubricant and debris increasing the wear rate and the degradation process of the oil at a micro-contact level. The results are in good agreement with the extensive work carried out by Varadi et al. where he used finite element models to estimate the generation of flash temperature within similar contact regimes [34] and with the analytical measurements carried out by Conte et al. [25]. The author could not identify any similar experimental approach, which matches well with the experimental and analytical result of such a contact within the literature. Additionally, a possible thermal deformation of the fibers was expected according to the flash temperature calculations which were close to the T_g (glass transition temperature) range of the fibers (1100±50 °C) [35]. A very good match of the calculated flash temperature results within the micro-asperity

contact with the SEM observations of the post-test MMMF calcium aluminosilicate fibers is revealed as it can be seen in (Section 5.2).

5. SEM observations of surface wear

5.1. Fibers wear damage

In order to analyze in a qualitative way the wear damage of the fibers, images of the worn fiber surfaces were observed by a scanning electron microscope Zeiss Supra 35VP and an optical microscope Olympus BX60. According to these observations, and as is cited by other authors [36,37] the various stages of fiber thinning, cutting, pulling-out, cracking and pulverization during post-test microscopy analysis across the wear surface of the contact path are shown in Fig. 12. Since the MMMF calcium aluminosilicate fibers are not crystalline in structure, they do not split longitudinally into thinner fibers but rather break transversely into shorter pieces [38] as shown in Fig. 12a. Additionally, the inherent brittleness and the high grindability of most of the reinforcement fibers, like the studied ones, result in rapid fiber damage under abrasive wear [39] or erosive wear [40].

In all the cases when the pressure and velocity increased, the friction force and consequently frictional heating is significantly increased. Specifically, in the case where roughness profile was at 0.5 and 0.7 μm an accelerative breakage in the interfacial region is observed, resulting in fibers removal. Many tiny fiber fragments in the size of a few nanometers were generated alleviating severe contact by introducing a third body mechanism with a positive rolling effect. During sliding contact the viscous flow of the composite facilitates the movement of these fragments effectively reducing the frictional coefficient, shear stress and contact temperature within the rubbing materials. Additionally it is believed that nano-debris is helpful to the formation of transfer films leading to lower wear rates [41]. In contrast, in the cases where roughness profile was at 0.125 and 0.25 μm the wear of the fibers is much smoother, the fibers are merely exposed to the surface and excessive fiber damage is restricted.

Moreover, in Fig. 12f, some tiny areas on top of the fiber depicted by blue color indicate chemical attack. Fiber reinforced polymers are vulnerable to chemical attack by many substances including lubricating oils and fuels [42]. Chemical attack in this particular contact happened due to the presence of water and fluorine generating hydrofluoric acid (HF) or by electrolysis of metal fluorides (MF and MF_4) generating tetrafluoremethane (CF_4) a strong chemical solvent. Hydrofluoridic acid as well as tetrafluoremethane (CF_4) attacks the surface of the sample close to the edges, causing fiber debonding which results in rapid wear of the polymer matrix [43].

5.2. Thermal effects on fibers

Frictional heating induced by the fibers generates a relatively high temperature in the vicinity of the bulk material. Thus, thermal softening of the polymer matrix aggravates fibers exposure on the polymer surface, accelerating wear due to an instant sliding contact with the asperities of the steel counterpart. Frictional heat not only alters temperature frictional characteristics of fibers but it also combines with surface fatigue effects to hasten microcracking and fiber thinning. Frictional heat causes cracks to form across the refractory fibers and combined wear of the fibers and metal may occur despite the large difference in the hardness of the two materials [41,44]. Additionally, due to the brittleness of the fibers, cracking from thermal stresses after rapid cooling can also occur leading to pulverization as a result of crack growth and convergence [45].

SEM observations on isolated fibers show that accumulative thermal effects can seriously affect fibers durability by modifying their shape. In Fig. 13, the profound effect of frictional heating on

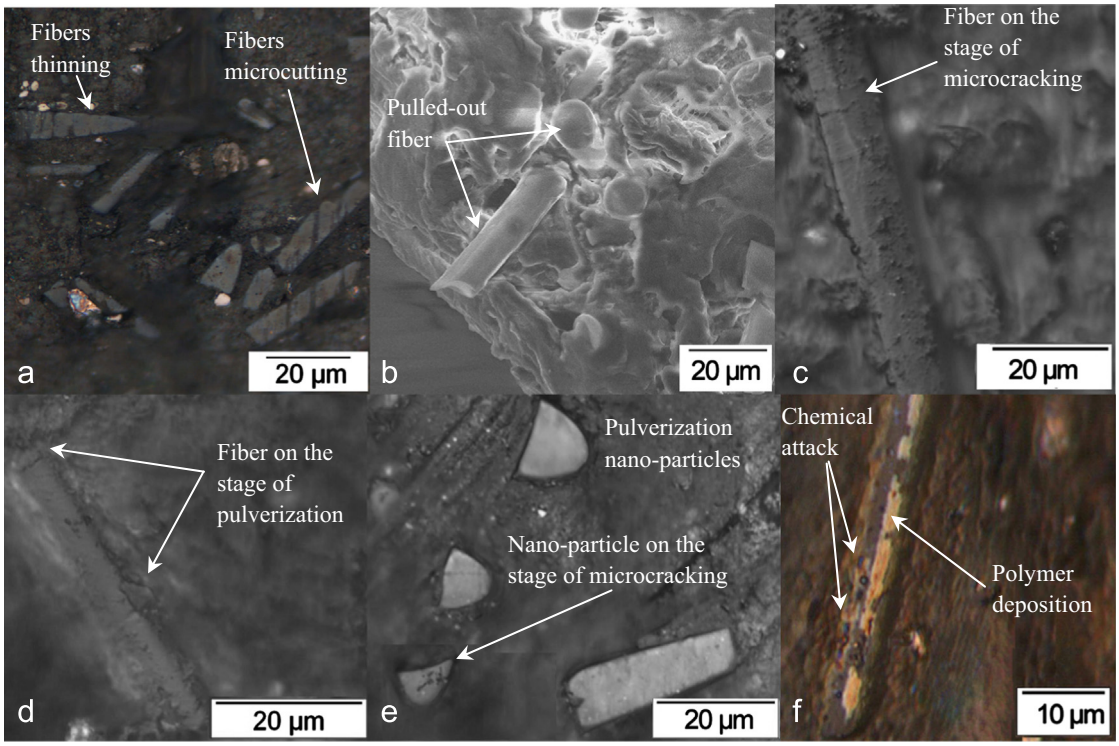

Fig. 12. Micrographs of wear mechanisms of fibers showing (a) fiber thinning and fracture, (b) pulled-out fiber from the matrix with worn elliptical tip, (c) fiber's microcracking, (d) pulverization incubation stage, (e) multiply microcutting and pulverization fiber deboning due to aggravating wear, and (f) chemical attack and polymer deposition across the fiber surface.

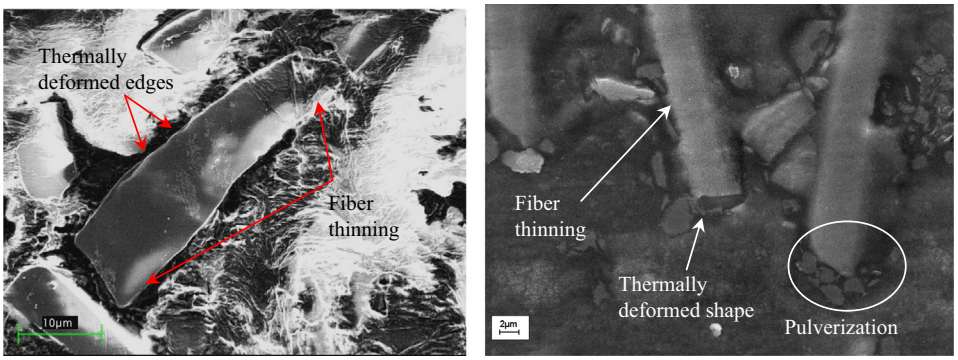

Fig. 13. Thermal and size deformation, contact wear fibers.

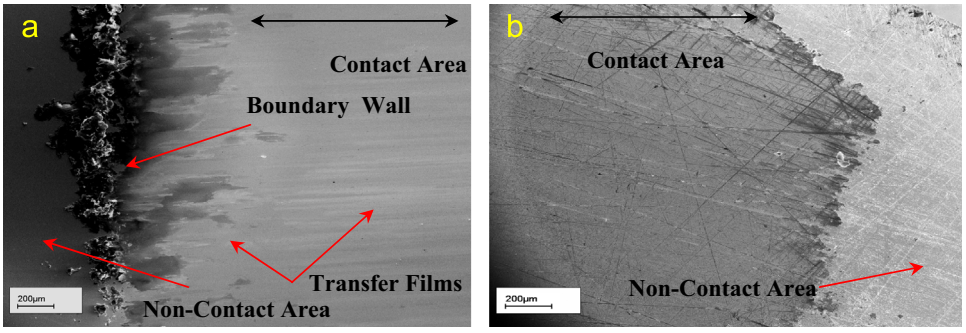

Fig. 14. Panoramic view of the transfer films across the steel samples: (a) Ra: 0.25 μm and (b) Ra: 0.7 μm.

an isolated fiber is illustrated. The edges across the fiber body are very smooth with an irregular undulation shape implying a thermal deformation process. Additionally fibers get thinner due to material removal while their size and diameter are significantly reduced. In Fig. 13a the thinner mechanism can be observed as the fiber from around 10 μm diameter in one edge it goes down to about 6 μm in the other edge. Thermal deformation effects are even more obvious in the case of Fig. 13b where a similar fiber experiences material loss due to the thinning process while consequently the round shape of the cylinder fiber is significantly deformed to an ellipsoidal shape by the synergic effect of thermal and squeezing mechanisms due to accumulative stresses. The thermal effects are noticeable affecting the performance and durability of fibers used for reinforcing polymer materials.

5.3. *Transfer films*

The sliding contact of the PTFE composite against the steel plate can produce contact temperatures capable of melting part of the polymer material under the conditions studied. This in turns forms a thin back transfer film on the worn surface of the steel plate. Transfer films develop due to the adhesion and interlocking of the polymer fragments into metal asperities during sliding [46]. In general wear it increases nonlinearly with the applied load and the sliding speed [33,47,48]. This nonlinear trend is mainly due to the trapped debris which alleviates the severity of the contact by introducing a third-particle, transfer films on the abrading surface and back transfer films to the rubbing surface of composite [47]. Furthermore, trapped debris and transfer of a polymer film to the abrading surface result in a clogging effect, which eventually mitigates the abrasion of material after few traverses [49].

The formation of transfer films across the steel plate is evaluated when the optimum (0.25 μm) and the poorest (0.7 μm) case scenario for the generation of contact temperatures is considered. In this study like in [4] clogging effect dominates the contact and many parallel transfer film layers with various thicknesses are formed across the steel plate (Fig. 14). In Figs. 14a and 15a where the roughness profile was at 0.25 μm the layers are firmly attached across the counterface. The formation of these polymer layers in correlation with the fact that in the edges of the sliding path a significantly thicker and higher layer of polymer is developed (Fig. 14a), creating an artificial boundary wall, indicates that radial leakage points within scroll expanders (Fig. 2b) can be significantly minimized and the tendency of the working fluid to flow through these areas is further confined. The adhesion performance in combination with the use of a less viscous lubricant is proved to be useful in increasing the performance and durability of the specific scroll unit [50]. In contrast in Figs. 14b and 15b where the roughness profile was at 0.7 μm, layers are discontinuous, more superficial and less dense restricting accumulation of the polymer material across the edges of the contact. Debris of the polymer is accumulated only on the highest surface asperities of the steel plate implying that a synergic effect of adhesion due to polymer melting and abrasion (shearing) due to penetration by the single and sharp asperities is taking place.

In Fig. 16 the formation of transfer films for 0.25 and 0.7 μm roughness profiles is shown with the use of a ZYGO interferometer. It is clear that for all the tested cases roughness displays a particular role. Interestingly it can be seen that in the case where roughness is in the range of 0.125–0.25 μm where the contact area is very smooth and the synergic effect by frictional heat is significant, the number of contact points with the counterface polymer material is increased forming continuous and dense transfer films. If roughness is in the range of 0.5–0.7 μm generating lower contact temperatures, transfer film layers are sporadic and discontinuous. Additionally the height difference between these two kinds of layers is significant. In the first case of 0.125–0.25 μm profile the average height is about 1 μm; however in the case

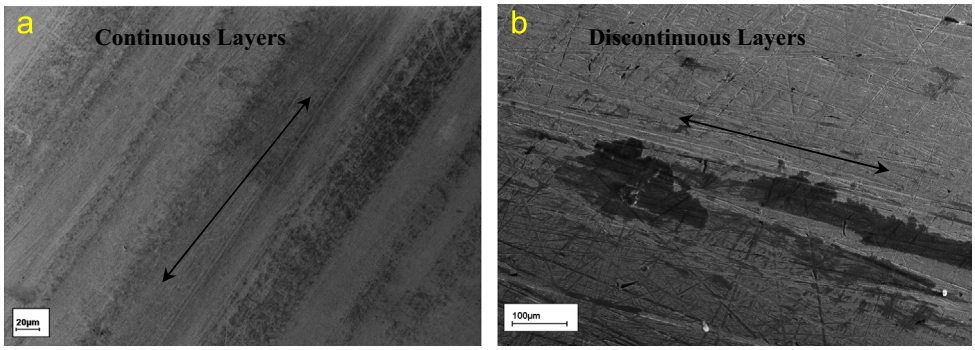

Fig. 15. Transfer films across the steel plate with different width and thickness profiles ordered in parallel formation to the sliding direction: (a) Ra: 0.25 µm and (b) Ra: 0.7 µm.

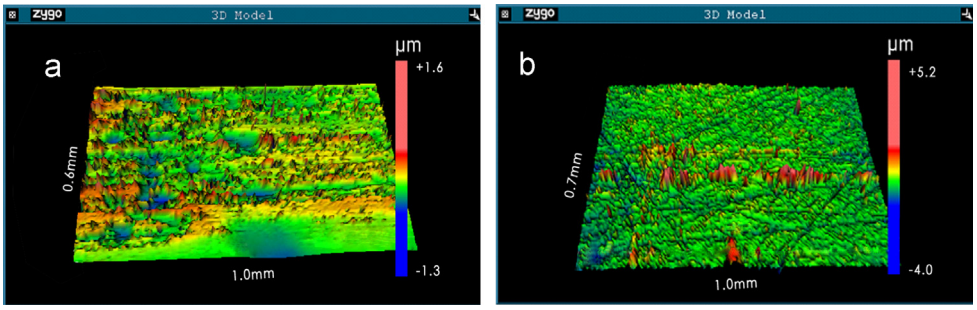

Fig. 16. Height and density of transfer films formed across the steel plate for two different cases: (a) Ra: 0.25 µm and (b) Ra: 0.7 µm.

where profile is at 0.5–0.7 µm average height can reach up to 5 µm. The reason for that is that the sharper and highest surface asperities of 0.5 and 0.7 µm profiles accumulate polymer material mainly across their tips. In contrast the blunt and more geometrically smoother asperities of 0.125 and 0.25 µm profiles accumulate more polymer material creating coherent transfer films.

6. Discussion

In the present study the contact temperature rise during the dry sliding contact of a PTFE composite against a high carbon steel plate was investigated with means of high precision thermal imagery using various combinations of sliding speeds 0.25 and 0.5 m/s, applied loads 10, 20, 30 and 40 N and Ra surface profiles 0.125, 0.25, 0.5 and 0.7 µm. The contact temperature on the studied sliding tribo-pair is the sum of ambient temperature, steady state frictional heating and transient friction temperature, which includes flash and interface temperatures as a function of the applied pressure, the sliding speed and the roughness profile.

It has been seen that for all the cases with the increment of the sliding velocity from 0.25 to 0.5 m/s heating zones are more concentrated and contact temperature as well as friction coefficient significantly increases. When sliding speed increases, the friction energy being dissipated is also increased. This is caused by the increment of the polymer's asperities impaction rate by the polished counterface, which resulted in a rapid increment of the adhesive friction and the temperature at the interface. Consequently, increased contact temperature affects the strain rate and shear strength (rate of deformation at the interface) of the adhesive junctions formed between the PTFE material and the steel counterface and friction coefficient increases. Moreover, an experimental assessment of the Bauschinger effect showed that the strain hardening and strength of polymers increase with the rate of deformation to which they are subjected [51]. Additionally according to Conte et al. [33], PTFE structure changes when it is heated up and a more compact structure is generated while Khedkar et al. [32] in their work showed that the higher the heat fusion values exhibited by PTFE composites during sliding, the higher the thermal stability at the interface. Thus, when sliding speed increases (rate of deformation at the interface), strain rate increases and consequently the strength of adhesive junctions formed between PTFE and the counterface also increases; hence there is an increase in friction.

With the increment of the applied pressure more asperities of the steel plate establish a contact with the composite PTFE leading to higher thermal deformation at the contact points. The contact temperature generally increases due to the larger contact area and the poor thermal diffusivity of the PTFE material. The generated frictional heat results in two antagonistic effects on the friction coefficient. On the one hand the shear strength of the PTFE composite decreases and thus so does the friction coefficient. On the other hand, the elastic modulus of the composite decreases, assisting the formation of multiple adhesion joints by the asperities impaction which resulted in more contact spots due to the larger contact area and then the friction coefficient increases. Therefore these two competitive aspects would determine the final friction coefficient. In the present study, the friction coefficient of the specific tribo-pair gradually decreases at higher applied loads since the decrease in shear strength is dominant and higher thermal stability is achieved while the contact temperature at the interface increases significantly. Thus, an increment of friction coefficient is not necessarily followed by an increment of the contact temperature for this particular contact regime. In lower applied loads, contact is restricted between the hard fibers and the steel asperities raising the friction coefficient, whereas in higher applied loads the viscoelastic performance of the polymer relaxes the severe contact regime and drops the friction coefficient. The abovementioned phenomenon is also explained in the work carried out by Tzanakis et al. [21] where similar materials were used for sliding friction tests.

In the cases where roughness profile was doubled from 0.125 to 0.25 µm, contact temperature is slightly increased. In contrast in

the cases where roughness profile was doubled from 0.25 to 0.5 μm, the contact temperature significantly dropped. Then as roughness increased from 0.5 to 0.7 μm the surface temperature regime was kept at similar levels. Interestingly there is an optimum surface roughness profile at 0.25 μm, which can seriously affect surface temperature gradient at the interface of the contact and achieve high contact temperatures. Specifically, when a lower roughness than 0.25 μm is used, contact temperature is reduced to about 17% while when higher roughness is used contact temperature is dropped to about 29%. Temperature fluctuation depends on two contrary effects. On one hand there is a drop in the temperature due to the fact that multiple continuous layers of polymer are formed across the counterface of the steel sample, creating a very soft substrate which dumps the heat effects and cools down the critical region. On the other hand since the thermal diffusivity of the bulk polymer material is low, heat is accumulated within the transfer films. In the case of surface profile at 0.125 μm where the morphology of the asperities on the steel plate (blunt asperities) is extremely smooth (larger contact area), temperature reduction is mainly derived from the fact that the number of contact points between the hard fibers and the exposed steel asperities is restricted since transfer layers interpose the severe contact alleviating thermal effects and minimizing hot-spots. In the case where roughness was at 0.25 μm a similar mechanism is involved as a semi-soft surface contact is observed; however friction coefficient is slightly higher. The friction component resulting from adhesion equaled the product of the real contact area and the contact between the hard fibers and the exposed steel asperities. In this particular case as hot-spots dominate the contact zone, elastic modulus of PTFE decreases (friction coefficient increases) and large amounts of frictional heat are accumulated within the sliding bodies and the transfer films. Thus a combination of contact points and transfer layers, according to their performance as cooling agents or accumulative heat sources, determines the final friction coefficient and contact temperature. In contrast, in the case where roughness is further increased (from 0.25 to 0.5 and to 0.7 μm) the contact is mainly isolated between the highest surface asperities indicating that severe contact is limited only in that contact area and shear strength governs this particular contact regime (friction coefficient decreases). Considerably higher transfer films are mainly formed across these contact points relaxing the contact and absorbing part of the heat. Additionally, the dissipation of frictional energy as heat and the conduction into the rubbing bodies is alleviated due to the surrounding air environment which is trapped within the contact bodies. The combination of polymer layers and convection by the cooler air medium alleviates thermal effects and significantly reduces the friction coefficient and the contact temperature of the interface.

The addition of fibers within the bulk material of the polymer is potentially useful to improve its tribological performance. However the flash temperature which is generated in the contact spots between the fibers and the counterface material is very high, accelerating the wear and thermal degradation of the polymer matrix and the fibers. Analytical results indicated high temperature regimes up to 1000 °C in some cases implying that fibers should have been affected or deformed in such temperatures. Moreover, microscopic observations of thermal deformed fibers have shown good agreement with the analytical flash temperature calculations of micro-asperity contact. In such high temperatures the interfacial toughness of the bulk material in the vicinity is reduced and the size of the interfacial crack increases. The reinforcement can be easily removed during abrasive wear conditions, especially in higher roughness profiles where asperities are sharper, and a negative reinforcement effect is observed [52]. Any portion of reinforcement that is removed as wear debris contributes to the overall frictional work rate of the material alleviating the contact. Additionally, pulverization of the exposed or removed fibers accumulates debris, which according its size can contribute to the reduction of the frictional coefficient and consequently of the frictional heat [53]. Thus, a positive rolling effect by nano- or micro-scale particles can improve friction regime by avoiding severe contact.

In all the test regimes transfer films were formed across the steel counterpart and produce adhesive wear mechanism which strongly affects the mitigation of the thermal effects. The determinant is that in the cases where the roughness of the steel plate was at 0.125 and 0.25 μm a rapid formation of stable transfer films is achieved. This is explained by the higher contact temperatures achieved among the lower roughness profiles and recorded by the thermal camera. Contact temperatures generate viscoelastic effects by melting parts of the polymer material. The deposition of the melted polymer across the asperities of the steel plate creates symmetric and continuous transfer films. In contrast in the cases where steel roughness was at 0.5 and 0.7 μm transfer films formation was constrained. Observations from the thermal camera showed that contact temperatures are significantly lower implying less vigorous viscoelastic behavior by the polymeric material. The formation of continuous and stable transfer films is restricted. Transfer films are mainly formed by shearing or seizure of the exposed asperities, which tend to gouge into the counterface of the polymer matrix. Consequently abrasion dominates across the polymer surface. This shearing mechanism can also be interpreted by the fact that friction coefficient is significantly lower compared to the 0.125 and 0.25 μm roughness profiles for the reason that the decrease in shear strength dominates the contact as discussed previously.

Finally it is also noticed that the tip seal during conditions of dry friction could be heated to a relatively high temperature, at nearly 120 °C. This testifies to the intensity of the process of friction energy dissipation. As far as the properties of PTFE composites depend strongly on temperature, a knowledge of the distribution of the thermal field in a seal component, like the studied tip seal of the scroll, will make it possible to model the shearing and stress mechanisms and most importantly to determine their viscoelastic behavior during the process of friction [13]. This in turn will improve the durability and sustainability of PTFE seals while the performance of advanced engines as scroll expanders will be enhanced. Engine losses will be minimized whereas a high-pressure ratio over the service period will be maintained.

7. Conclusions

The following conclusions can be drawn from the present study:

1. Thermal contact regime of the specific sliding contact is a combination of surface roughness, sliding velocity, applied load, debris size and transfer films. A good correlation of the experimental findings with the analytical results has been achieved.
2. Friction coefficient increases with the sliding speed and is substantially reduced with the increment of the applied load whereas contact temperature increases with the increment of both the parameters.
3. An ultra-fine or a very rough surface of the steel material sample alleviates thermal effects. The contact with Ra roughness profile at 0.25 μm achieves the highest temperatures followed by the contact with 0.125 μm whereas the contacts with 0.5 and 0.7 μm generate the lowest frictional temperatures.
4. The most influential parameter for the surface temperature rise within the specific contact is the sliding velocity. The impact

the sliding velocity has on the specific contact can be up to 51% in contrast to the applied load and the surface roughness which are both significantly lower.
5. A reasonable correlation between the rate of frictional work and the contact temperature rise during sliding was observed experimentally and the influence of the roughness on the actual contact temperature regime is highlighted.
6. Flash temperatures generated in the fibers/steel plate contact can reach up to 1000 °C. Thermal effects are noticeable as SEM micrographs revealed, affecting the performance and durability of calcium aluminosilicate fibers.

Additional remarks

The formation of continuous transfer films across the steel counterpart with Ra at 0.125 and 0.25 μm and the development of artificial barriers in the edges of the sliding path indicate that radial leakage points (Fig. 2b) within scroll expanders can be significantly minimized and their efficiency can be improved. Smoother steel plate profiles can be extremely beneficial for scroll expander applications or similar turbine units in order to minimize the tendency of the working fluid to escape. An oil free configuration can also be considered. Additionally, a detailed determination of the morphology of transfer films in order to analyze the physical parameters and mechanisms that guide the frictional process and dominate the generation of contact temperatures will be examined in future studies.

Acknowledgments

The authors would like to thank the Experimental Techniques Center (ETC) in Brunel University and especially Dr. Lorna Anguilano for her valuable contribution in the chemical characterization of the PTFE composite materials.

References

[1] I. Tzanakis, M. Hadfield, A. Georgoulas, N. Kotsovinos, Cavitation damage observations within scroll expander lubrication systems, WIT Transactions on Engineering Sciences 66 (2010) 261–272.
[2] I. Tzanakis, M. Hadfield, Z. Khan, Durability of domestic scroll compressor systems, WIT Transactions on Engineering Sciences 62 (2009) 229–240.
[3] F.E. Kennedy, X. Tian, The effect of interfacial temperature on friction and wear of thermoplastics in the thermal control regime, Tribology Series 27 (C) (1994) 235–244.
[4] I. Tzanakis, N. Garland, M. Hadfield, Cavitation damage incubation with typical fluids applied to a scroll expander system, Tribology International 44 (12) (2011) 1668–1678.
[5] M. Kalin, Influence of flash temperatures on the tribological behaviour in low-speed sliding: a review, Materials Science and Engineering A 374 (1–2) (2004) 390–397.
[6] P. Stempflé, O. Pantalé, T. Djilali, R.K. Njiwa, X. Bourrat, J. Takadoum, Evaluation of the real contact area in three-body dry friction by micro-thermal analysis, Tribology International 43 (10) (2010) 1794–1805.
[7] G. Sutter, N. Ranc, Flash temperature measurement during dry friction process at high sliding speed, Wear 268 (11–12) (2010) 1237–1242.
[8] P.N. Bogdanovich, D.V. Tkachuk, Temperature distribution over contact area and "hot spots" in rubbing solid contact, Tribology International 39 (11) (2006) 1355–1360.
[9] G. Straffelini, M. Pellizzari, L. Maines, Effect on sliding speed and contact pressure on the oxidative wear of austempered ductile iron, Wear 270 (9–10) (2011) 714–719.
[10] P. Baranowski, K. Damziak, J. Malachowski, L. Mazurkiewicz, M. Kastek, T. Piatkowski, H. Polakowski, Experimental and numerical tests of thermo-mechanical processes occurring on brake pad lining surfaces, WIT Transactions on Engineering Sciences 71 (2011) 15–24.
[11] M. Ingram, T. Reddyhoff, H.A. Spikes, Thermal behaviour of a slipping weat clutch, Tribology Letters 41 (1) (2011) 23–32.
[12] J.M. Degrange, M. Thomine, P. Kapsa, J.M. Pelletier, L. Chazeau, G. Vigier, G. Dudrange, L. Guerbe, Influence of viscoelasticity on the tribological behaviour of carbon black filled nitrile rubber (NRB) for tip seal application, Wear 259 (1–6) (2005) 684–692.
[13] W. Wieleba, The role of internal friction in the process of energy dissipation during PTFE composite sliding against steel, Wear 258 (5–6) (2005) 870–876.
[14] L. Chang, K. Friedrich, Enhancement effect of nanoparticles on the sliding wear of short fiber-reinforced polymer composites: a critical discussion of wear mechanisms, Tribology International 43 (12) (2010) 2355–2364.
[15] G.M. Bartenev, V.V. Lavrentev, Friction and Wear of Polymers, Elsevier, Amsterdam, 1981, p. 212.
[16] B.N.J. Persson, Rubber friction: role of the flash temperature, Journal of Physics: Condensed Matter 18 (32) (2006) 7789–7823.
[17] D. Guha, S.K. Roy Chowdhuri, The effect of surface roughness on the temperature at the contact between sliding bodies, Wear 197 (1–2) (1996) 63–73.
[18] L. Chang, K. Friedrich, Enhancement effect of nanoparticles on the sliding wear of short fiber-reinforced polymer composites: a critical discussion of wear mechanisms, Tribology International 43 (12) (2010) 2355–2364.
[19] F.J. Martínez, M. Canales, J.M. Bielsa, M.A. Jiménez, Relationship between wear rate and mechanical fatigue in sliding TPU-metal contacts, Wear 268 (2–3) (2010) 388–398.
[20] J.K. Lancaster, Estimation of the limiting PV relationships for thermoplastic bearing materials, Tribology 4 (2) (1971) 82–86.
[21] I. Tzanakis, M. Hadfield, I. Hensaw, N. Garland, Z. Khan, Experimental sliding performance of composite tip seal with high-carbon steel plate under lubricated conditions applied to scroll expander systems, Tribology Transactions 54 (4) (2011) 505–513.
[22] F.P. Bowden, D. Tabor, The Friction and Lubrication of Solids, Clarendon Press, Oxford, 1964.
[23] A.M.A. Mohamad Altaweel, C. Ranganathaiah, B. Siddramaiah, Positron lifetime spectroscopy and differential scanning calorimetric study of polystyrene-based composites with fly ash, cenospheres, and calcium aluminosilicate as fillers, Journal of Applied Polymer Science 16 (2010) 3087–3094.
[24] M.L. Baesso, A.C. Bento, A.R. Duarte, A.M. Neto, L.C.M. Miranda, J.A. Sampaio, T. Catunda, S. Gama3, F.C.G. Gandra, Nd_2O_3 doped low silica calcium aluminosilicate glasses: thermomechanical properties, Journal of Applied Physics 85 (1999) 8112–8118.
[25] M. Conte, B. Fernandez, A. Igartua, Frictional heating calculations based on tailored experimental tests. in: Proceedings of the Nordic Tribology 2012 Conference, Trondheim, Norway, June 12–15th 2012.
[26] I. Tzanakis ,M. Hadfield, Evaluation of flash temperatures of a composite elastomer with dry sliding conditions in contact with high carbon steel, in: Proceedings of the 10th International Conference on Surface Effects and Contact Mechanics: Computational Methods and Experiments, Malta, 21–23 September 2011.
[27] H. Blok, Theoretical study of temperature rise at surfaces of actual contactn under oilness lubrication conditions, Institution of Mechanical Engineers General Discussion on Lubrication 2 (1937) 222–235.
[28] J.C. Jaeger, Moving sources of heat and temperature at sliding contacts, Proceedings of the Royal Society of New South wales 76 (1942) 203–224.
[29] M.F. Ashby, J. Abulawi, H.S. Kong, On Surface Temperatures at Dry Sliding Surfaces, Cambridge University Press, Cambridge, UK, 1997.
[30] X. Tian, F.E. Kennedy, Maximum and average flash temperatures in sliding contacts, ASME Journal of Tribology 116 (1994) 167–174.
[31] T.A. Stolarski, A system for wear prediction in lubricated sliding contacts, Lubrication Science 8 (1996) 315–350.
[32] J. Khedkar, I. Negulescu, E.I. Meletis, Sliding wear behavior of PTFE composites, Wear 252 (2002) 361–369.
[33] Conte M., B. Fernandez, A. Igartua, Effect of surface temperature on tribological behavior of PTFE composites, in: Proceedings of the Surface Effects and Contact Mechanics X, WIT press, UK, 2011, pp. 219–230.
[34] K. Varadi, Z. Neder, K. Friedrich, FE contact and thermal analysis of composite surfaces with different fiber orientations subjected to a sliding steel asperity, Finite Elements in Analysis and Design 40 (2004) 1475–1497.
[35] L. Cornier, D.R. Neuville, G. Callas, Relation between structure and glass transition temperature in low-silica calcium aluminosilicate glasses: the origin of the anomaly of low silica content, Journal of the American Ceramic Society 88 (2005) 2292–2299.
[36] L. Chang, Z. Zhang, Tribological properties of epoxy nanocomposites Part II. A combinative effect of short carbon fiber with nano-TiO_2, Wear 260 (2006) 869–878.
[37] J. Bijwe, Wear failures of reinforced polymers, in: R.J. Shipley, W.T. Becker (Eds.), ASM Handbook, Vol. 11: Failure Analysis and Prevention, ASM International, 2002. ISBN: 0871707047, 9780871707048.
[38] Man-Made Vitreous Fibers, Navy Environmental Health Center, Norfolk, Virginia, 1997, 23513-2617 〈http://www-nehc.med.navy.mil/downloads/IH/MMVF.pdf〉.
[39] J. Bijwe, C.M. Logani, U.S. Tewari, Influence of fillers and fiber reinforcement on abrasive wear resistance of some polymeric composites, Wear 138 (1990) 77–92.
[40] P.J. Mathias, W. Wu, K.C. Goretta, J.L. Routbort, D.P. Groppi, K.R. Karasek, Solid particle erosion of a graphite-fiber-reinforced bismaleimide polymer composite, Wear 135 (1989) 161–169.
[41] T.A. Libsch, P.C. Becker, S.K. Rhee, Friction and wear of toughened ceramics against steel, in: Proceedings of the JSLE International Tribology Conference, Tokyo, Japan, Elsevier, 8–10 July 1985, pp. 185–190.

[42] J.K. Lancaster, Composites for aerospace dry bearing applications, in: K. Friedrich (Ed.), Friction and Wear of Polymer Composites, Elsevier, Amsterdam, 1986, pp. 363–397.
[43] D.C. Evans, Polymer–fluid interactions in relation to Wear, in: D. Dowson, M. Godet, C.M. Taylor (Eds.), Proceedings of the 3rd Leeds-Lyon Symposium on Tribology, Wear of Non-Metallic Materials, September 1976, Institution of Mechanical Engineers Publisher, London, 1978, pp.47–71.
[44] G.M. Carter, R.M. Hooper, J.L. Henshall, M.O. Guillou, Friction of metal sliders on toughened zirconia ceramic between 298 and 973 K, Wear 148 (1991) 147–160.
[45] G.W. Stachowiak, A.W. Batchelor, Engineering Tribology, 2nd ed., Butterworth-Heinemann, Jordan Hill, Oxford, 2001.
[46] S. Bahadur, The development of transfer layers and their role in polymer tribology, Wear 245 (2000) 92–99.
[47] N.S.M. El-Tayeb, Two-body abrasive behaviour of untreated SC and R-G fibers polyester composites, Wear 266 (2009) 220–232.
[48] M. Conte, Effect of fillers on tribological properties of PTFE composites, in: Proceedings of the Ecotrib 2011 Conference, Wien, 2011.
[49] N.S.M. El-Tayeb, B.F. Yousif, Evaluation of glass fiber reinforced polyester composite for multi-pass abrasive wear applications, Wear 262 (2007) 1140–1151.
[50] I. Tzanakis, M. Hadfield, B. Thomas, S.M. Noya, S. Austen, I. Hensaw, Future perspectives on sustainable tribology, Renewable and Sustainable Energy Reviews 16 (6) (2012) 4126–4140.
[51] D.J.A. Senden, J.A.W. Dommelen, L.E. Govaert, Strain hardening and its relation to Bauschinger effects in oriented polymers, Journal of Polymer Science, Part B: Polymer Physics, 48 (2010) 1483–1494.
[52] Y. Lee, C.K.H. Dharan, R.O. Ritchie, A physically-based abrasive wear model for composite materials, Wear 252 (2002) 322–331.
[53] L. Chang, Z. Zhang, C. Breidt, K. Friedrich, Tribological properties of epoxy nanocomposites I. Enhancement of the wear resistance by nano-TiO_2 particles, Wear 258 (2005) 141–148.